Supporting Information

Section S1 – Large area and single particle composition (EDX), crystallinity (XRD) and size analysis (TEM) of CrFeCoNiCu nanoparticles via LAL

Table S1: Large area composition of crystalline CrFeCoNi**Cu** HEA NPs via ps-LAL, determined via STEM-EDX by evaluating three different positions of the STEM sample with average values and standard deviations.

	Cr [at%]	Fe [at%]	Co [at%]	Ni [at%]	Cu [at%]
Position 1	20.4	22.0	22.6	22.7	12.3
Position 2	21.6	20.9	21.4	22.2	13.8
Position 3	21.6	22.9	22.6	21.3	11.6
Average	**21.2**	**21.9**	**22.2**	**22.1**	**12.6**
Standard Deviation	0.57	0.82	0.57	0.58	0.91

Table S2: Large area composition of amorphous CrFeCoNi**Cu** HEA NPs via ns-LAL, determined via STEM-EDX by evaluating three different positions of the STEM sample with average values and standard deviations.

	Cr [at%]	Fe [at%]	Co [at%]	Ni [at%]	Cu [at%]
Position 1	20.9	21.2	20.7	20.3	16.9
Position 2	21.8	20.2	19.8	20.1	18.1
Position 3	19.7	19.3	18.6	20.1	22.4
Average	**20.8**	**20.2**	**19.7**	**20.2**	**19.1**
Standard Deviation	0.86	0.78	0.86	0.09	2.36

Table S3: Single-particle composition of crystalline CrFeCoNi**Cu** HEA NPs of various sizes via ps-LAL, determined by STEM-EDX.

Particle No.	Particle Diameter [nm]	Cr [at%]	Fe [at%]	Co [at%]	Ni [at%]	Cu [at%]
1	8	25.7	20.6	24.5	18.3	11.0
2	11	23.9	20.6	21.0	25.1	9.3
3	19	26.5	18.2	21.9	25.3	8.1
4	21	23.2	25.8	24.1	18.1	8.8
5	23	24.7	21.7	23.1	24.8	5.7
6	24	21.1	22.0	23.3	21.4	12.2
7	24	15.7	16.7	14.1	20.7	32.8
8	25	24.0	19.6	20.1	20.33	16.0
9	26	19.0	19.5	17.5	23.2	20.9
10	26	12.7	16.3	18.1	19.4	33.49
11	30	20.6	24.2	22.5	22.6	10.2
12	53	23.1	23.2	23.4	21.3	8.9
13	66	19.4	22.8	23.5	22.0	12.3
Average		**21.5**	**20.9**	**21.3**	**21.7**	**14.6**
Standard Deviation		3.9	2.7	3.0	2.3	8.72

Table S4: Single-particle composition of amorphous CrFeCoNi**Cu** HEA NPs of various sizes via ns-LAL, determined by STEM-EDX.

Particle No.	Particle Diameter [nm]	Cr [at%]	Fe [at%]	Co [at%]	Ni [at%]	Cu [at%]
1	7	13.5	19.8	13.6	21.3	31.4
2	11	29.5	24.8	18.8	20.3	6.6
3	14	24.2	21.0	20.5	22.7	11.7
4	14	25.0	22.2	19.7	22.6	10.5
5	15	16.9	18.1	18.8	23.0	23.2
6	16	21.2	19.2	19.3	24.6	15.7
7	19	31.0	23.2	21.7	18.2	5.9
8	24	26.7	23.3	22.4	21.2	6.4
9	25	26.2	23.6	22.4	20.7	7.2
10	26	20.1	23.6	22.8	26.1	7.4
11	27	28.5	24.2	23.8	19.0	4.5
12	29	22.5	22.4	22.0	23.9	9.2
13	130	19.8	18.9	17.3	20.5	23.6
Average		**23.5**	**21.9**	**20.2**	**21.9**	**12.6**
Standard Deviation		4.9	2.1	2.7	2.2	8.1

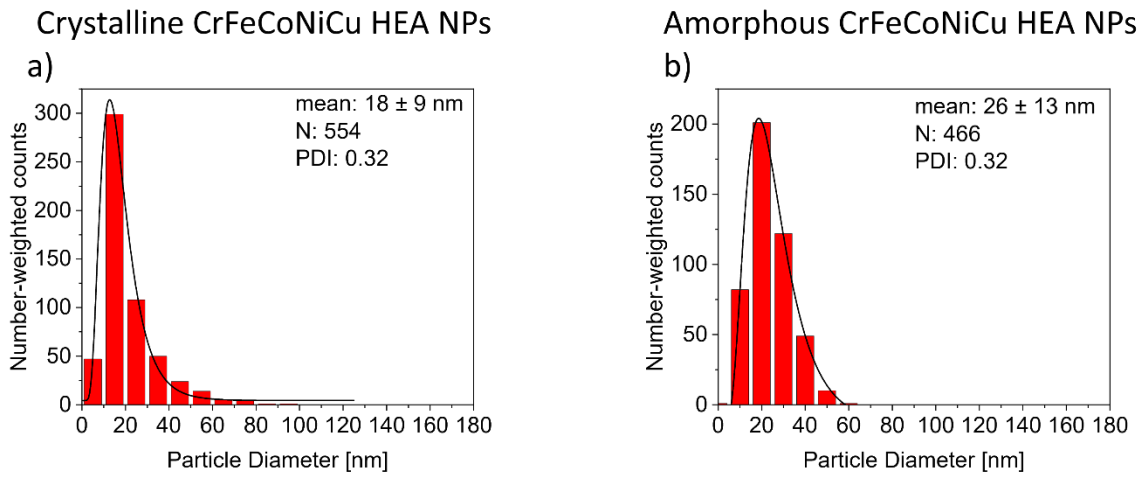

Figure S1: Number-weighted particle size distributions of crystalline (a) and amorphous (b) CrFeCoNiCu HEA NPs, determined by evaluation of TEM images of multiple hundred NPs with given mean diameters, number of counted HEA NPs (N), polydispersity index (PDI).

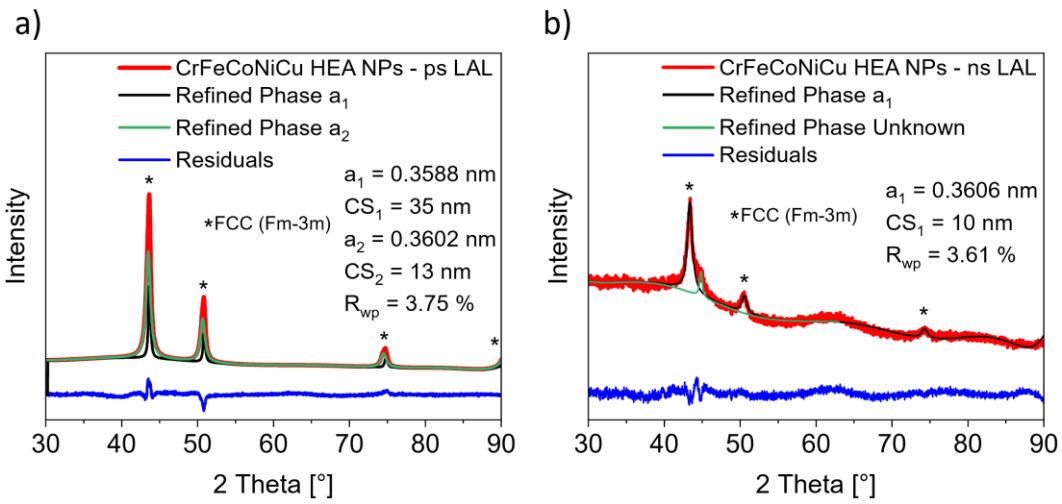

Figure S2: Structural analysis of LAL-generated CrFeCoNiCu HEA NPs via ps-LAL (a) and ns-LAL (b). In addition to Figure 1 of the main manuscript, this figure displays the calculated values for lattice parameters (a) and average crystallite sizes (CS), derived from Rietveld refinements of the raw X-ray diffraction data.

Section S2 – Compositional and structural characterization of sintered CrFeCoNiCu HEA bulk target

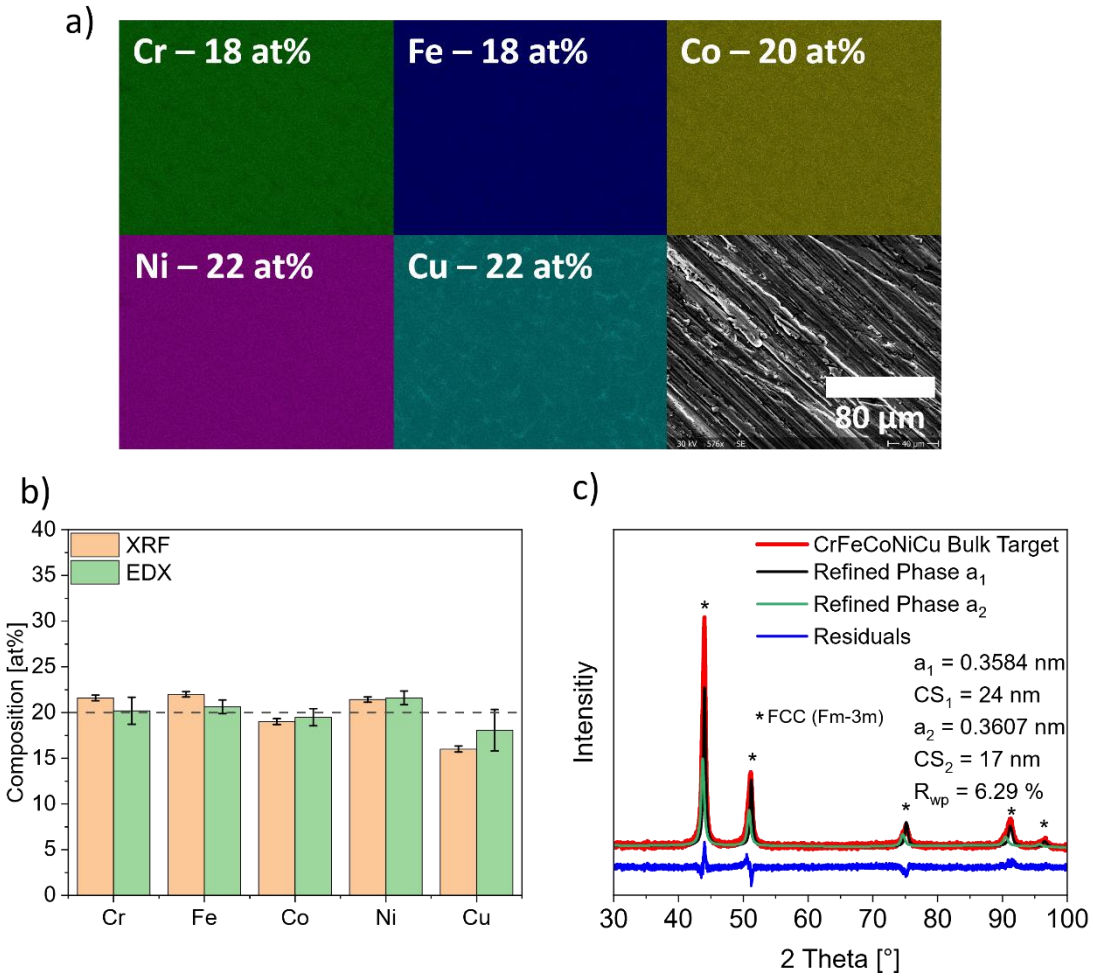

Figure S3: Compositional and structural analysis of the CrFeCoNiCu bulk target, fabricated by spark sintering. (a) SEM-EDX map of individual Cr, Fe, Co, Ni, and Cu elemental distribution and compositional value within an area of 0.032 mm². (b) Composition of the bulk target's surface, evaluated by conducting XRF and EDX analysis, with all values and error bars determined by three (XRF) and five (EDX) individual measurements of different target areas. (c) X-ray diffraction pattern showing a fcc structure and Rietveld refinements with refined values for lattice parameters (a) and crystallite sizes (CS), consisting of two distinct lattice constants (a_1 = 0.3584 nm and a_2 = 0.3607 nm), consistent with minor segregation shown in (a).

Section S3 – Compositional and structural analysis of high-entropy alloy microparticles via high-energy ball milling

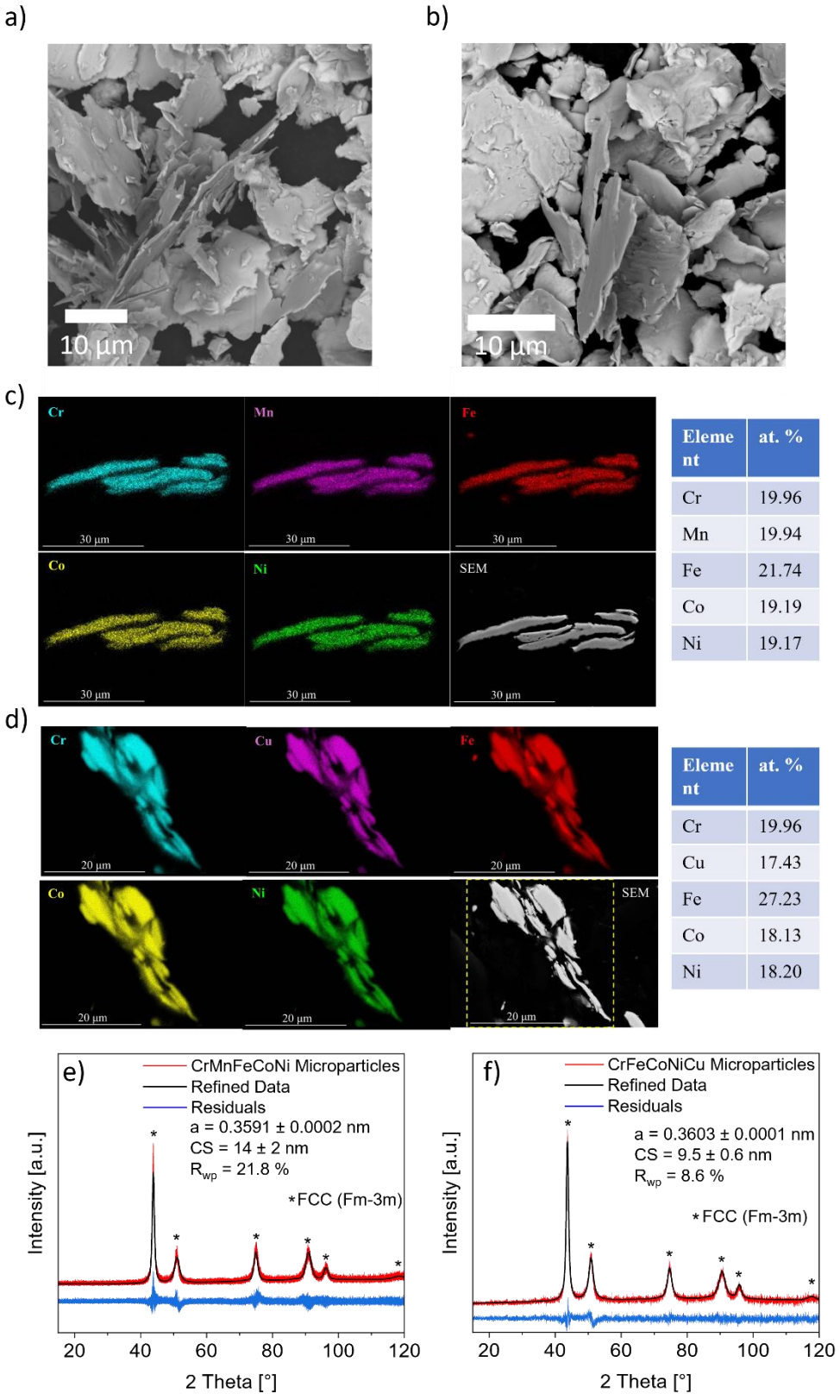

Element	at. %
Cr	19.96
Mn	19.94
Fe	21.74
Co	19.19
Ni	19.17

Element	at. %
Cr	19.96
Cu	17.43
Fe	27.23
Co	18.13
Ni	18.20

Figure S2: Characterization of high-entropy alloy microparticles via high-energy ball milling (HEBM). (a) and (b): Exemplary SEM images of plate-shaped HEA microparticles. (c) and (d): Cross sections of selected microparticles, showing elemental homogeneity and values of CrMnFeCoNi (a) and CrFeCoNiCu (b) microparticles. X-ray diffraction patterns depict a single-phase fcc structure in both CrMnFeCoNi (c) and CrFeCoNiCu (d) microparticles, with refined values for lattice parameter (a) and average crystallite size (CS) displayed in conjunction with refinements in the figures.

Section S4 – STEM-EDX analysis of high-entropy alloy nanoparticles via laser-fragmentation in liquid

Table S5: Large area composition of CrMnFeCoNi HEA NPs via MP-LFL, determined via STEM-EDX by evaluating three different positions of the sample with average values and standard deviations.

	Cr [at%]	Mn [at%]	Fe [at%]	Co [at%]	Ni [at%]
Position 1	17.1	28.9	25.0	13.8	15.2
Position 2	20.1	31.0	21.5	13.8	13.7
Position 3	18.1	34.1	22.0	12.6	13.2
Average	**18.4**	**31.3**	**22.8**	**13.4**	**14.0**
Standard Deviation	1.25	2.14	1.55	0.57	0.85

Table S6: Large area composition of CrFeCoNiCu HEA NPs via MP-LFL, determined via STEM-EDX by evaluating three different positions of the sample with average values and standard deviations.

	Cr [at%]	Fe [at%]	Co [at%]	Ni [at%]	Cu [at%]
Position 1	18.8	21.6	17.3	21.9	20.4
Position 2	19.5	27.3	16.3	17.2	19.7
Position 3	21.4	28.3	15.3	14.8	20.1
Average	**19.9**	**25.7**	**16.3**	**18.0**	**20.1**
Standard Deviation	1.10	2.95	0.82	2.95	0.29

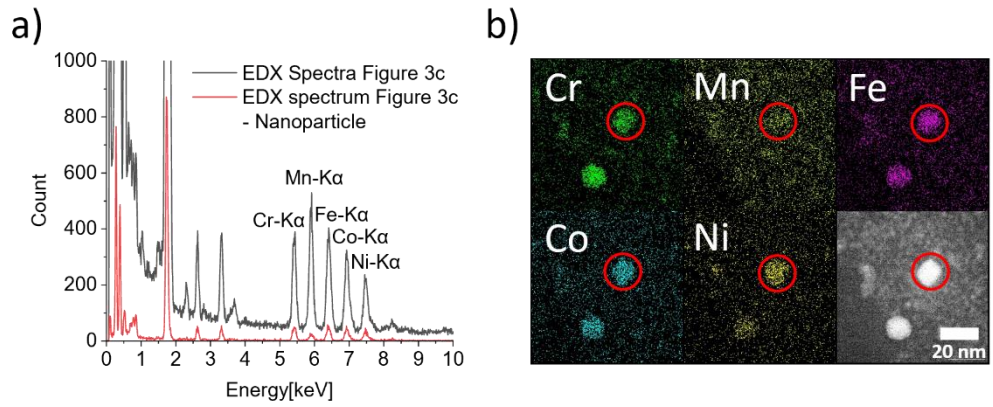

Figure S3: (a) Exemplary global EDX spectrum (black) and spectrum of an individual CrMnFeCoNi HEA NP (red) via MP-LFL. (b) EDX map from Figure 3c, highlighting the nanoparticle that is shown in the red EDX spectrum in (a).

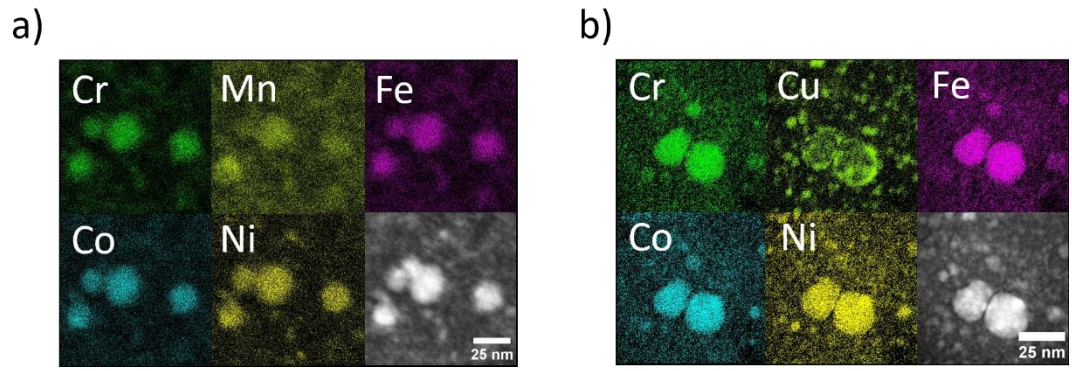

Figure S4: STEM-EDX maps of high-entropy alloy nanoparticles fabricated via laser-fragmentation in ethanol: (a) CrMnFeCoNi and (b) CrFeCoNiCu. This figure highlights the structure and composition of NPs that exceed the mean diameter of the sample (CrMnFeCoNi: 10 ± 4 nm and CrFeCoNiCu: 8 ± 3 nm) and shows partial segregation of Cr-Cu within a single NP.

Section S5 – Structural and compositional characterization of crystalline and amorphous CrMnFeCoNi HEA NPs for electrochemical investigations

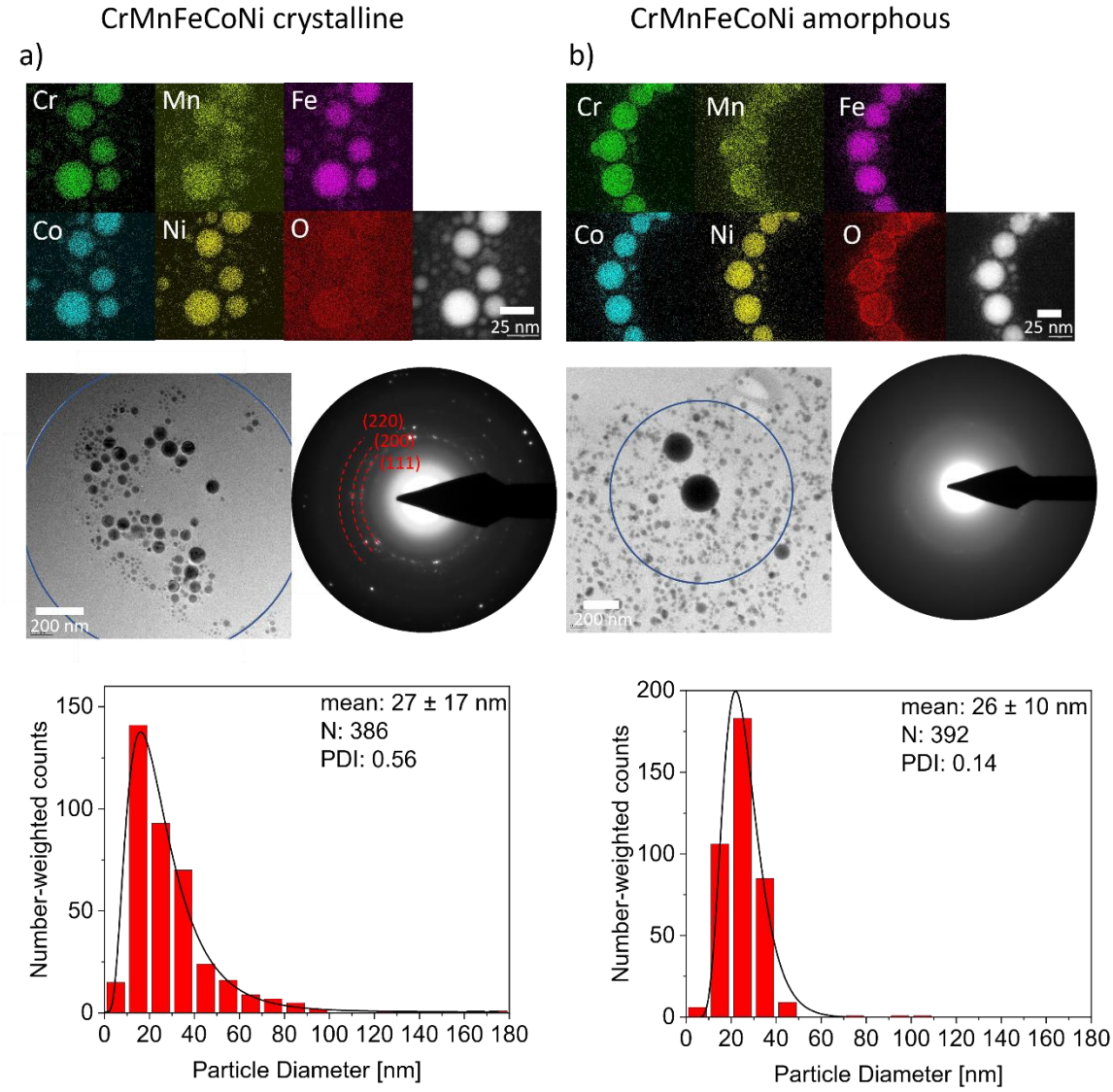

Figure S5: Characterization of CrMnFeCoNi HEA NPs for electrochemical investigations, analogously fabricated as described in the experimental section and an earlier study.[1] Compositional (STEM-EDX) and structural (SAED) analysis as well as particle size histograms of crystalline CrMnFeCoNi HEA NPs via ps-LAL (a) and amorphous CrMnFeCoNi HEA NPs via ns-LAL (b), both synthesized in ethanol. Size histograms show mean diameters, number of analyzed particles (N) and polydispersity index (PDI) were replotted from Ref. 1.

Section S6 – X-ray photoelectron analysis of electrochemically (un)treated high-entropy alloy nanoparticles.

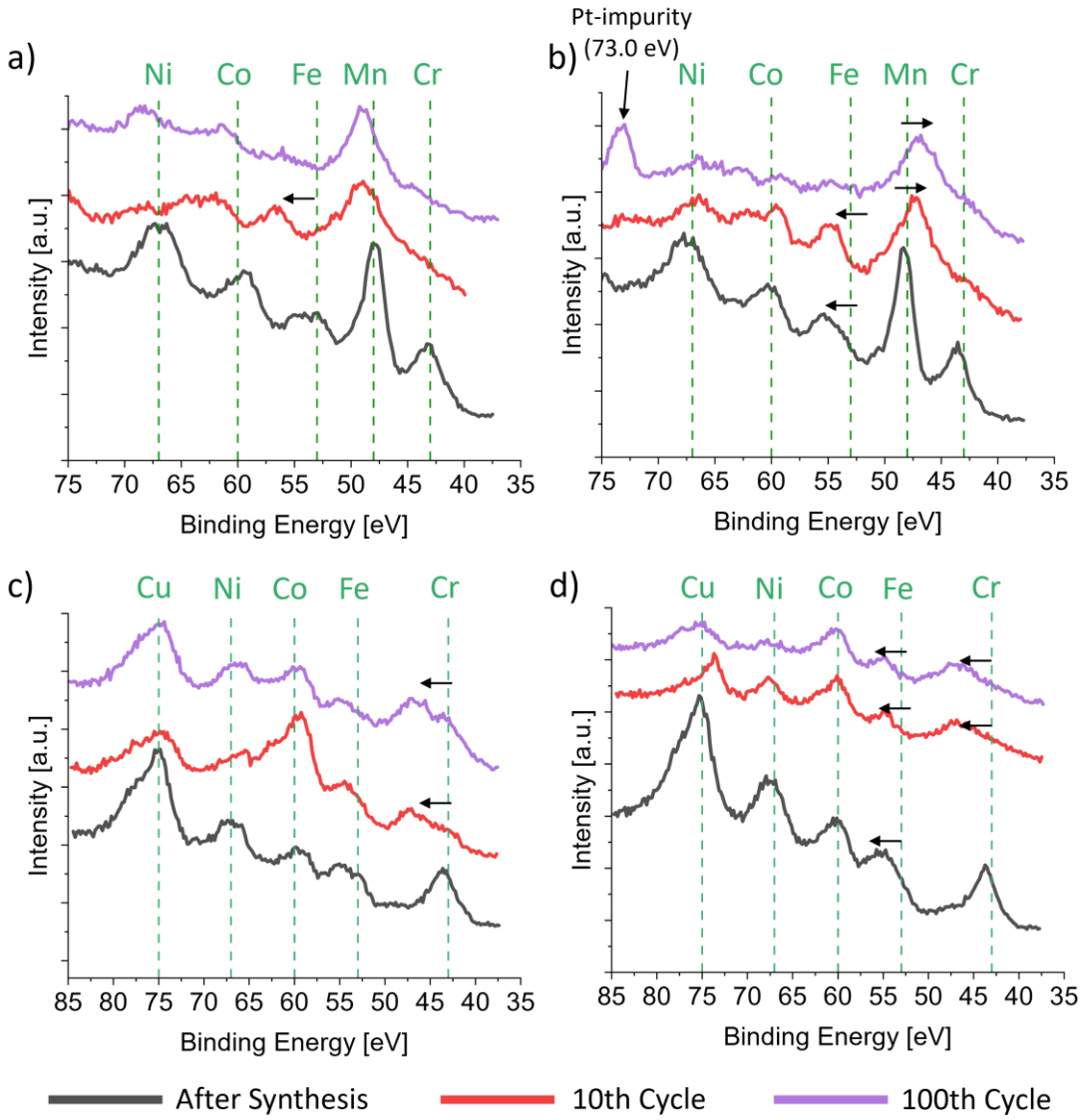

Figure S6: XPS spectra of electrochemically untreated (after synthesis) and treated (10th cycle, 100th cycle) HEA NPs, displaying 3p regions of all metals. (a) Crystalline CrMnFeCoNi HEA NPs, (b) amorphous CrMnFeCoNi HEA NPs, (c) Crystalline CrFeCoNiCu HEA NPs, and (d) Amorphous CrFeCoNiCu HEA NPs. Green dashed lines indicate literature values of 3p photoelectron peaks of each individual element, and black arrows hint towards shifts in binding energy as described elsewhere.[2]

Table S7: Compositional values of all metals analyzed via XPS in Figure S6. The values have been determined by fitting each individual peak using a Shirley-type background and asymmetric Lorentzian curve.

Crystalline CrMnFeCoNi HEA NPs					
	Cr [at%]	Mn [at%]	Fe [at%]	Co [at%]	Ni [at%]
After Synthesis	19.79	46.29	7.4	9.6	16.92
10th Cycle	0	75.83	12.34	9.73	2.1
100thCylce	0	81.68	0	7.5	10.82
Amorphous CrMnFeCoNi HEA NPs					
	Cr [at%]	Mn [at%]	Fe [at%]	Co [at%]	Ni [at%]
After Synthesis	22.39	44.54	11.40	7.48	14.19
10th Cycle	0	70.37	12.68	10.04	6.92
100thCylce	0	87.12	4.91	4.06	3.91
Crystalline CrFeCoNiCu HEA NPs					
	Cr [at%]	Fe [at%]	Co [at%]	Ni [at%]	Cu [at%]
After Synthesis	39.78	13.41	7.61	10.12	29.09
10th Cycle	43.54	9.14	31.10	2.55	13.66
100thCylce	60.41	4.73	8.56	5.07	21.21
Amorphous CrFeCoNiCu HEA NPs					
	Cr [at%]	Fe [at%]	Co [at%]	Ni [at%]	Cu [at%]
After Synthesis	38.12	14.52	9.27	12.38	25.71
10th Cycle	36.93	1.58	30.99	12.91	17.58
100thCylce	58.08	7.43	18.94	2.31	13.23

Section S7 – Linear sweep voltammetry for activity evaluation of the oxygen evolution reaction of high-entropy alloy nanoparticles surfaces.

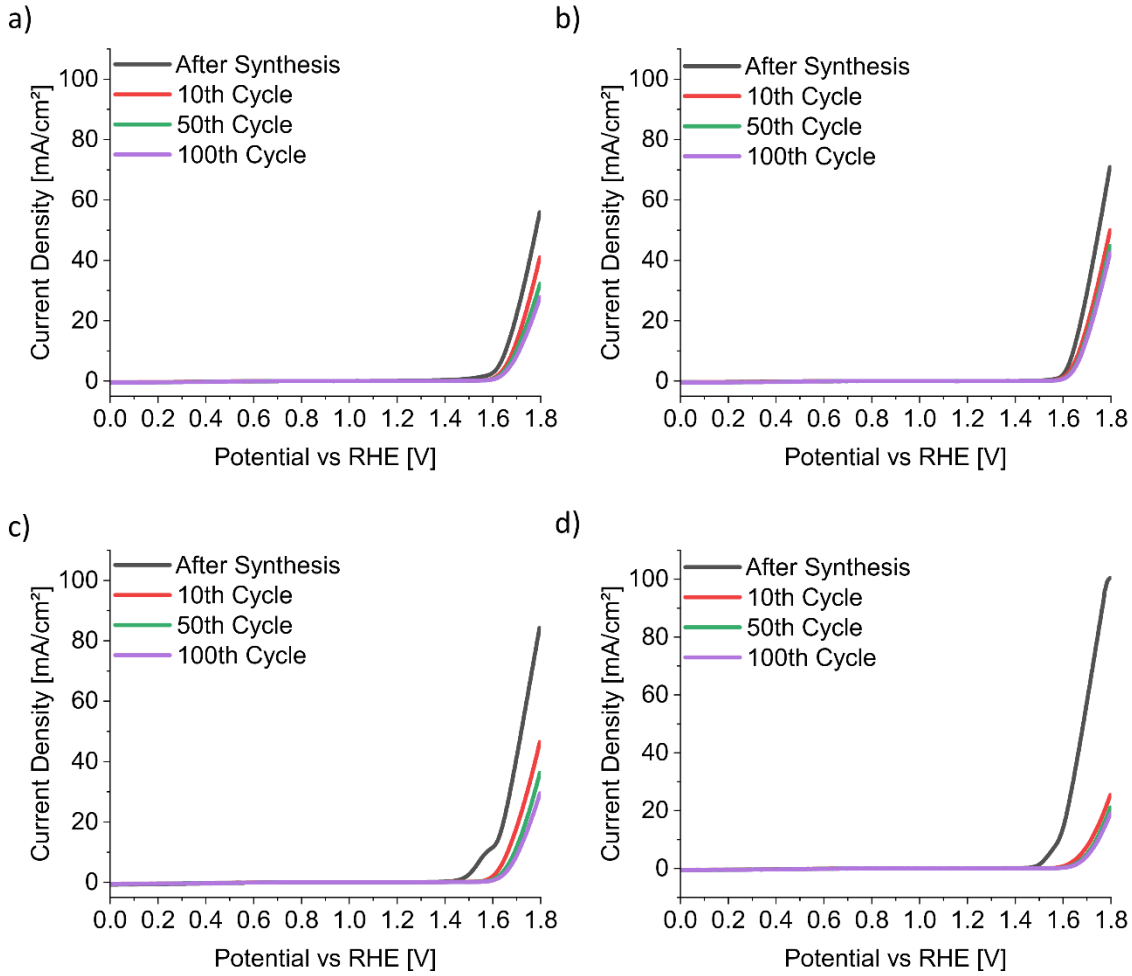

Figure S7: Linear sweep voltammetry of HEA NPs in the potential window 0 – 1.8 V vs. RHE, displaying activity in oxygen evolution reaction. (a) Crystalline CrMnFeCoNi NPs, (b) amorphous CrMnFeCoNi NPs, (c) crystalline CrFeCoNiCu NPs, and (d) amorphous CrFeCoNiCu NPs.

Section S8 – Electrochemical impedance spectroscopy for evaluation of resistance in high-entropy alloy nanoparticles during oxygen evolution reaction.

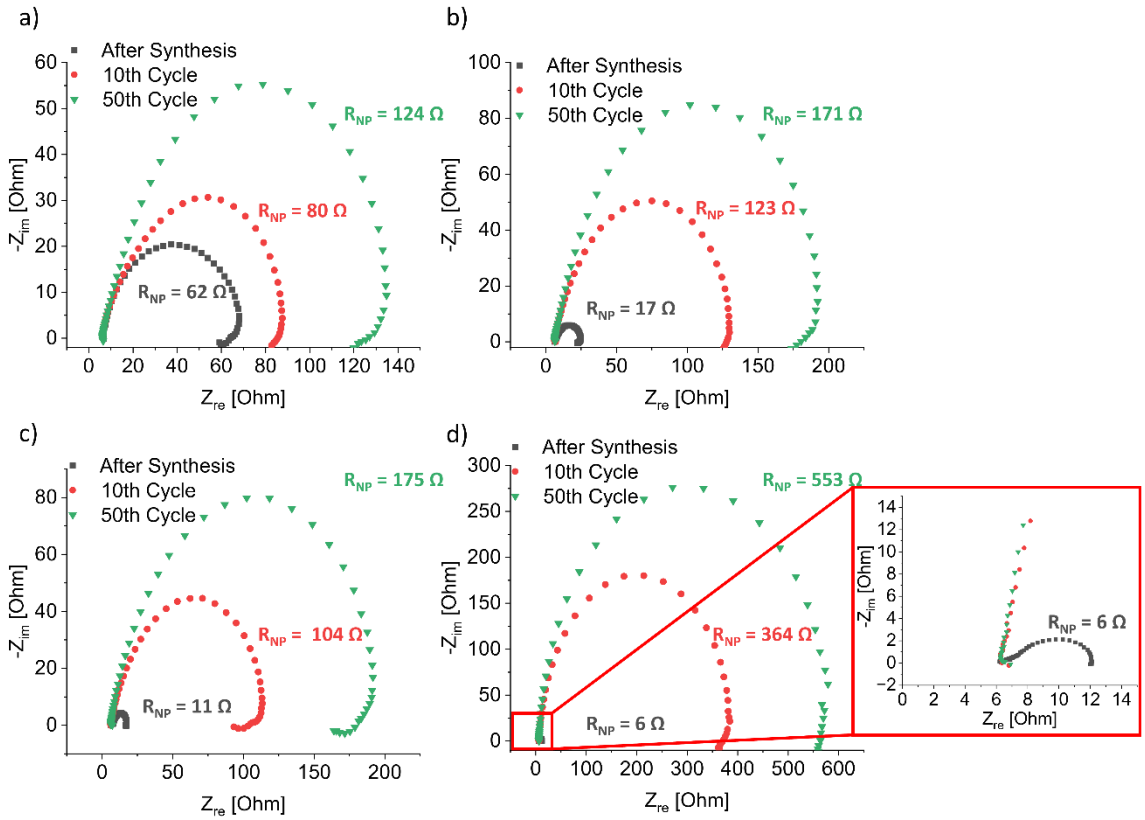

Figure S8: EIS measurements of high-entropy alloy nanoparticles during OER at 1.6 V vs. RHE and frequencies of 0.1 Hz – 100 kHz with given nanoparticle resistances (R_{NP}) next to each EIS measurement after respective cycles of cyclic voltammetry (0 (= After Synthesis), 10, and 50). (a) Crystalline CrMnFeCoNi NPs, (b) amorphous CrMnFeCoNi NPs, (c) crystalline CrFeCoNiCu NPs, and (d) amorphous CrFeCoNiCu NPs with inset of lower resistance region. Note that axis scales differ in each diagram for a better overview.

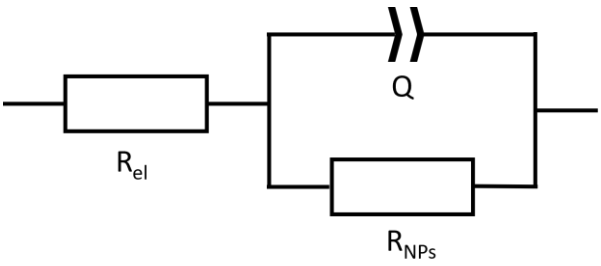

Figure S9: Model circuit for fitting electrochemical impedance data to determine resistances of HEA NPs. R_{el} = Resistance electrolyte, R_{NPs} = resistance HEA NPs, Q = constant phase element.

Section S9 – Specific surface area of high-entropy alloy nanoparticles via BET analysis

Table S8: Summary of measured values of specific surface areas (SSA) of crystalline (C) and amorphous (A) high-entropy alloy nanoparticles, determined by physisorption of nitrogen and evaluating with the BET model.

	C-CrMnFeCoNi	A-CrMnFeCoNi	C-CrFeCoNiCu	A-CrFeCoNiCu
SSA [m^2/g]	37.45	34.24	31.91	1.78

References

1 R. Stuckert, F. Pohl, O. Prymak, U. Schürmann, C. Rehbock, L. Kienle and S. Barcikowski, *Beilstein J. Nanotechnol.*, 2025, accepted.

2 H. Zhu, S. Sun, J. Hao, Z. Zhuang, S. Zhang, T. Wang, Q. Kang, S. Lu, X. Wang, F. Lai, T. Liu, G. Gao, M. Du and D. Wang, *Energy Environ. Sci.*, 2023, **16**, 619–628, https://pubs.rsc.org/en/content/articlelanding/2023/ee/d2ee03185j.